Scanning Microscopy

Volume 3 | Number 1 Article 28

12-10-1988

Observations of Colloidal Gold Labelled Platelet Microtubules: High Voltage Electron Microscopy and Low Voltage-High Resolution Scanning Electron Microscopy

R. M. Albrecht
University of Wisconsin, Madison

J. Prudent
University of Wisconsin, Madison

S. R. Simmons
University of Wisconsin, Madison

J. Pawley
University of Wisconsin, Madison

J. J. Choate
Loyola University

Scanning Microscopy, Vol. 3, No. 1, 1989 (Pages 273-278) 0891-7035/89$3.00+.00
Scanning Microscopy International, Chicago (AMF O'Hare), IL 60666 USA

OBSERVATIONS OF COLLOIDAL GOLD LABELLED PLATELET MICROTUBULES: HIGH VOLTAGE ELECTRON MICROSCOPY AND LOW VOLTAGE-HIGH RESOLUTION SCANNING ELECTRON MICROSCOPY

R.M. Albrecht,[1*] J. Prudent,[1] S.R. Simmons,[1] J. Pawley,[2] and J.J. Choate[3,4]

[1] Department of Veterinary Science, University of Wisconsin, Madison, WI 53706

[2] Department of Zoology and the Integrated Microscope Resource, University of Wisconsin, Madison, WI 53706

[3] Heinz VA Hospital and Loyola University, Maywood, IL 60153

[4] Present Address, Kaiser Permanente Medical Center, Santa Clara, CA 95051

(Received for publication March 12, 1988, and in revised form December 10, 1988)

Abstract

18 nm colloidal gold-antitubulin and 4 nm colloidal gold-antitubulin were used to label microtubules in adherent, fully spread platelets. Both sizes of marker effectively labelled microtubules in the partially extracted platelets. However only the 4 nm gold penetrated the dense microfilament matrix of the inner filamentous zone so that portions of microtubules within this cytoskeletal zone could be tracked. The gold marker could be visualized well with 1 MeV high voltage transmission EM and with 5 kV or greater secondary imaging or 20 kV backscattered imaging of carbon only coated samples. 1 kV secondary imaging permitted high resolution imaging of the surface of tubules and the microfilaments with their respective associated material. Individual gold-antibody complexes were difficult to identify by shape alone due to the tendency of the antibody coats to blend together when in very close approximation and due to the presence of other molecules or molecular aggregates similar in size to the gold-antibody labels.

Microtubules were seen to wind in and out of the inner and outer filamentous zones as they encircled the granulomere. Some tubules were seen to "dead end" at the peripheral web. Numerous smaller microtubule loops were present principally in the outer filamentous zone and tubules could be followed as they went from the outer filamentous zone through the inner filamentous zone and into the granulomere.

Key Words: Platelets, microtubules, cytoskeleton, low voltage high-resolution scanning electron microscope, colloidal gold, electron microscopy.

*Address for correspondence:

R.M. Albrecht
Department of Veterinary Science
University of Wisconsin
1655 Linden Drive
Madison, Wisconsin 53706
Phone No.: (608) 263-4162

Introduction

Colloidal gold-ligand or colloidal gold-antibody complexes have proven to be useful markers for light microscopy, transmission electron microscopy, and scanning electron microscopy (1,2,4,5,6,7,9,11,13, 16,17,23). This stems, in part, from their regular spherical shape, density, and size (3,7,22). We have previously utilized an approach combining conventional scanning electron microscopy (SEM) and high voltage transmission electron microscopy (HVEM) of whole, unsectioned platelets to view, respectively, the relationship of ligand labelled or antibody-gold labelled, surface glycoprotein molecules with the subjacent cytoplasmic cytoskeletal structure (4,11,13,16).

In fully spread platelets, the organization of microfilaments can be divided into 4 structurally distinct zones (12). The organization of microtubules is less distinct and it is difficult to follow their exact course, even in the whole platelet preparations, due to limited microtubule numbers and due to the density of the actin network through which the tubules traverse. Previous studies have suggested the peripheral microtubule band present in discoid platelets either 1. constricts around centralized platelet granules in the adherent fully spread platelets or 2. may depolymerize and reassemble in new locations 2 to 4 minutes later as the platelets adhere and spread (10,14,15,21,24).

Materials and Methods

To more clearly delineate the microtubule network, monoclonal antitubulin was directly conjugated to 18 nm and 4 nm colloidal gold and then used to label Formvar adherent, fully spread, human platelets (13).

The platelets were prepared by a modification of the fixation/extraction procedure of Langanger, et al (8,9). The extracted, pre-fixed platelets were labelled for up to 8 hours in the anti-tubulin-gold in a Tris buffered saline 0.1% bovine serum albumin (BSA) buffer. Longer labelling times did not affect label density (17). Following labelling, samples were washed and fixed in 0.1 M HEPES buffered 0.05% $Os0_4$ for 15 minutes. Samples were then washed and stained with aqueous 1% uranyl acetate for 15 minutes. Specimen dehydration was through a graded alcohol series to 100% ethanol itself dried by storage over molecular sieve. Samples were dried by the critical point procedure, alcohol as intermediate fluid and liquid CO_2 as transitional fluid, and observed either uncoated or after coating with a thin carbon layer by indirect

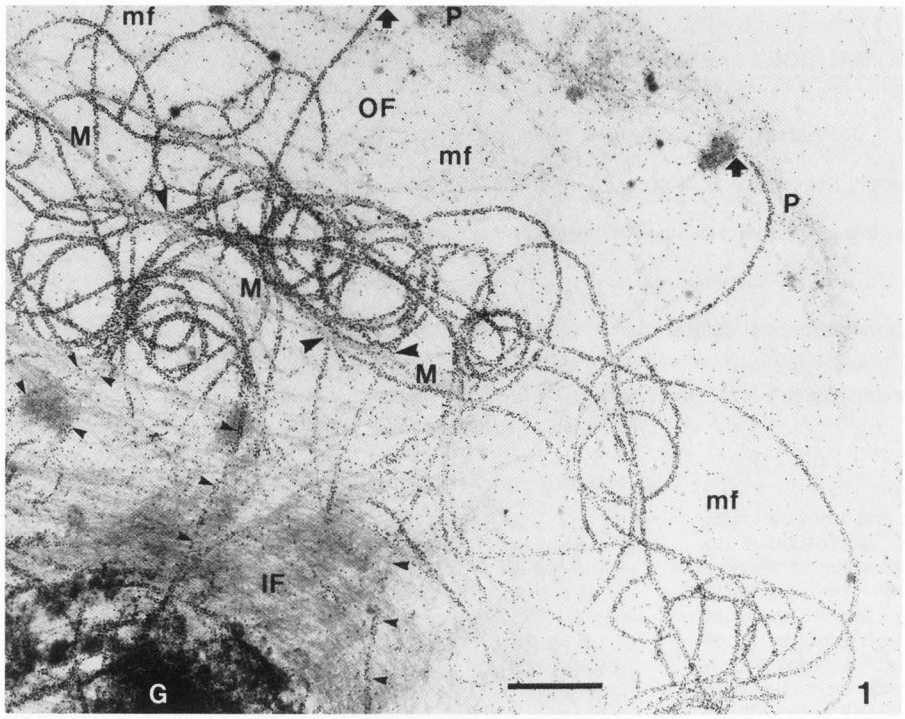

Figure 1.
HVEM of an adherent fully spread platelet. 18 nm colloidal gold-antitubulin can be seen labelling microtubules as they traverse the inner (IF) and outer (OF) filamentous zones. Occasional tubules terminate (short arrows) at the peripheral web (P). Tubules and tubule loops are well labelled in the outer filamentous zone where they pass through a more open microfilament network (mf). Labelling is reduced (large arrow heads) as tubules pass through microfilament bundles (M) in the outer zone. Labelling is also reduced or absent (small arrow heads) on tubules in the dense microfilament matrix of the inner zone. Labelling is again apparent on tubules in the granulomere (G) where the microfilament network is similar to that of the outer filamentous zone. Bar = 1.0 μm.

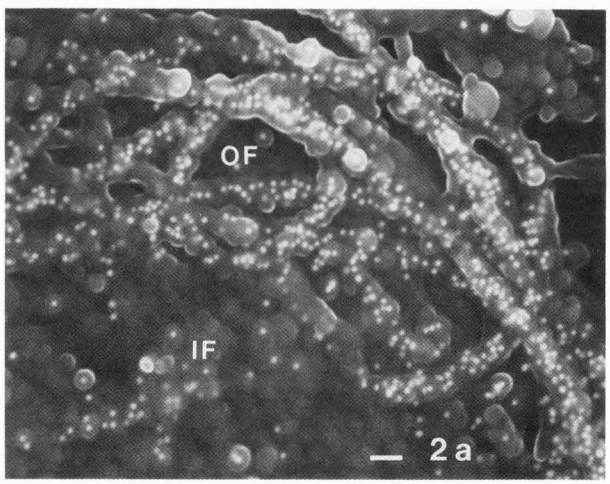

Figure 2a. LV-HR-SEM of 18 nm gold-antitubulin. Secondary electron image at 5.0 kV accelerating voltage. Tubules (arrows) in the outer filamentous zone (OF) are well labelled and the label is clearly visible. As in figure 1, once the tubules enter the dense actin meshwork of the inner filamentous zone (IF) labelling becomes spotty. Bar = 0.1 μm.

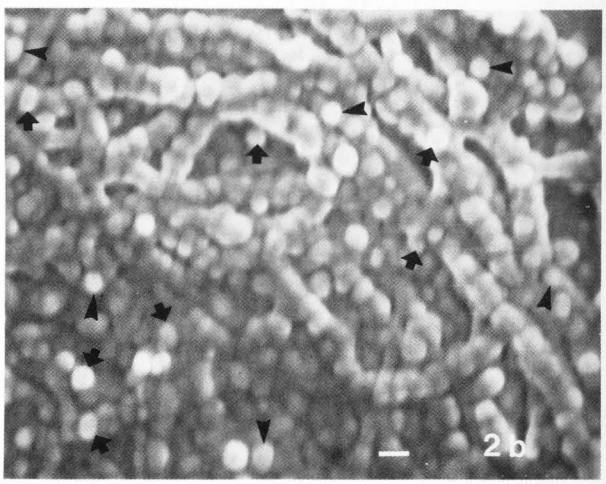

Figure 2b. LV-HR-SEM of 18 nm gold-antitubulin. Secondary electron image at 1 kV accelerating voltage. This is the same area as in figure 2a. The reduced accelerating voltage results in minimal primary beam penetration of the carbon coated specimen. The majority of the signal arises from the surface and hence surface features are more clearly imaged. The protein surface of the gold labels can be seen (arrows) but no Z contrast from the gold core is evident (compare with figure 2a). Positive identification of gold-antibody labels is difficult due to other proteins or protein aggregates of similar shape and size (arrow heads) and the tendency of the antibody coat of the gold labels to blend together when labels are in very close approximation. Bar = 0.1 μm.

evaporation. Labelled, dried platelets were observed both by HVEM, 1000 kV accelerating voltage (AEI-EM7) and by low-voltage high-resolution scanning electron microscopy (Hitachi S 900) at 1 kV and 5 kV accelerating voltages (18,19,20). The same specimen could be examined and reexamined by both forms of microscopy since metallic coating is not an absolute requirement when using the low voltage SEM. Samples were prepared on finder grids to facilitate location of individual platelets so that the same platelet could be viewed by HVEM and SEM.

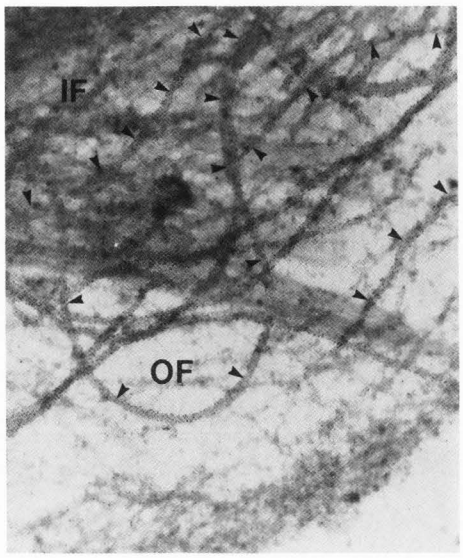

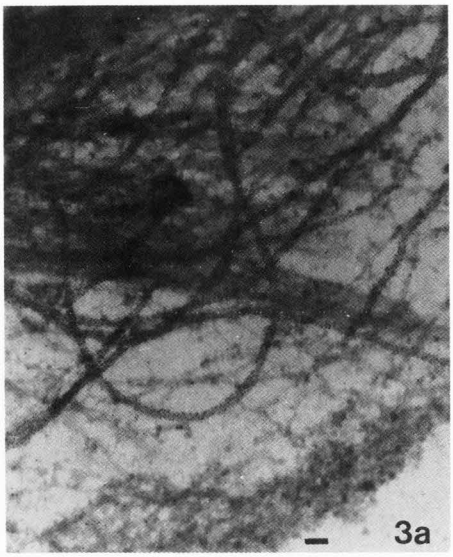

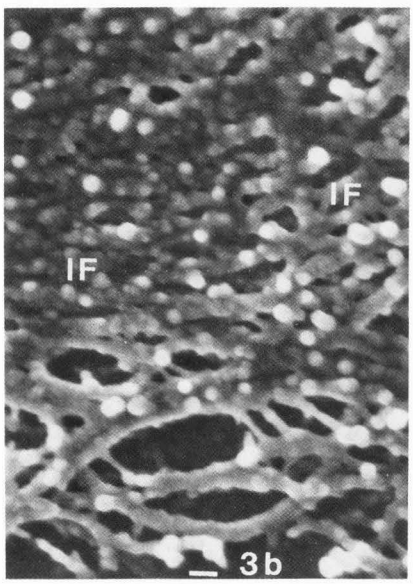

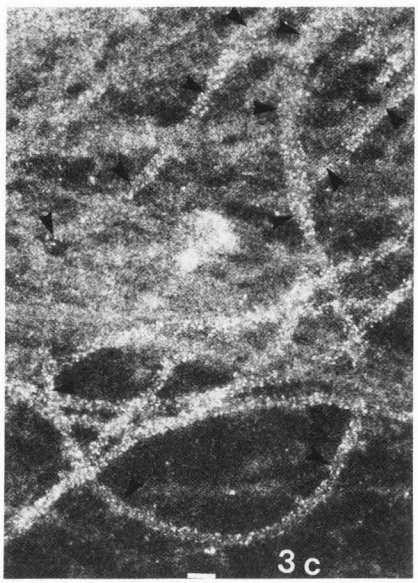

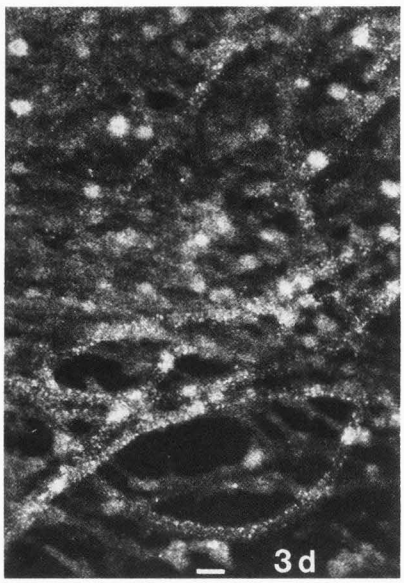

Figure 3a. HVEM stereo-pair of 4.0 nm gold antitubulin labelled platelets. The course of the microtubules (arrow heads) can be followed through both the outer filamentous zone (OF) and, in contrast to the 18 nm size label (see figures 1 and 2) also through the dense microfilament matrix of the inner zone (IF). The small 4.0 nm labels appear able to penetrate into the IF meshwork. Bar = 0.1 μm.

Figure 3b. LV-HR-SEM of 4.0 nm gold-antitubulin. This is a secondary image at 1.0 kV accelerating voltage of the same area seen in figure 3a. As in figure 2b the low accelerating voltage permits detailed imaging of the surface. The dense nature of inner filamentous zone (IF) microfilament matrix, composed of actin filaments and filament associated material is apparent. This matrix acts as a barrier to the 18 nm gold antibody label (approximately 34 nm total diameter antibody and gold) while the smaller 4.0 nm gold-antibody (approximately 8.0 nm total diameter) can penetrate in sufficient concentration to label most, but not all, portions of tubules within the matrix. Bar = 0.1 μm.

Figure 3c. LV-HR-SEM of 4.0 nm gold-antitubulin labelled platelet. Same area as seen in figures 3a and 3b. This is a backscattered electron image at 20 kV accelerating voltage. Surface detail is not apparent but strong Z contrast accentuates the gold particles enabling tracking of the labelled microtubules (arrows) both outside of and within the microfilament matrix. As with the 1 MeV HVEM transmission image tubules can be followed whether outside of or within the microfilament matrix. Bar = 0.1 μm.

Figure 3d. Combined 20 kV BEI and 1 kV secondary image can be used to follow labelled microtubules relative to the surface ultrastructure. Bar = 0.1 μm.

Results and Discussion

Colloidal gold labels of 4 and 18 nm can be readily visualized both by HVEM and by LV-HR-SEM. The HVEM, 1000 kV accelerating voltage, demonstrates the distribution of the gold labelled microtubules as they proceed in a generally circumferential path winding in and out of the outer and inner filamentous zones (Figure 1). Numerous smaller tight loops are formed as the tubules circle back on themselves (Figure 1). The uranium stained, more open microfilament network of the outer filamentous zone can be differentiated from the very dense microfilament network of the inner filamentous zone (Figure 1). Microfilament bundles are also visible as they traverse the outer filamentous zone (Figure 1). With the larger 18 nm gold, labelling diminishes significantly as the tubules enter regions of densely packed microfilaments (Figure 1). Occasionally a uranium stained tubule is visible among the dense microfilaments but little label is attached. LV-HR-SEM also demonstrates the pattern of labelled tubules. At higher accelerating voltage, 2 kV and above, the increased penetration of the primary electrons and the superior 2° electron emission characteristics of the gold result in high contrast between the biological material and the gold (Figure 2a). At lower accelerating voltages, 1.5-1.0 kV, the decreased penetration of the primary beam results in signal being collected from at or very near the surface (Figure 2b). As a consequence, the larger gold labels at the surface can be distinguished only by their shape and hence may be difficult to differentiate from other molecular species or aggregates of similar size and shape that may be present. Subsurface gold cannot be seen (Figure 2b). Labelling with the 3.5 to 4.0 nm gold label results in substantially less diminution in labelling density as these conjugates appear sufficiently small to penetrate the actin filament meshwork (Figure 3a). The dense meshwork pattern of actin filaments and lightly stained filament-associated-material, poorly visualized by HVEM, is readily visible with low 1.0 to 1.5 kV SEM accelerating voltage (Figure 3b) while the Z contrast generated by backscattered imaging at 20 kV permits identification of individual labels (Figure 3c). (Overlays of the 5 kV secondary image or 20 kV backscattered image, particularly in the case of metal coated specimens, are useful to show subsurface label in relation to surface structure and to differentiate label from other similarly sized and shaped structures. Figure 3d).

The HVEM and LV-HR-SEM are complimentary and can be used to advantage to demonstrate distribution of unlabelled and colloidal gold labelled cytoskeletal elements in whole cell preparations.

These studies in combination with correlative video enhanced DIC light microscopy, VDIC-LM, of unlabelled microtubules in living platelets (Choate, Prudent, and Albrecht, in preparation) have demonstrated several important features of platelet microtubule reorganization. As previously shown by White and Rao, constriction of preexisting circumferential microtubule bands appears to occur in a proportion of the platelets (24). However, the radial pattern of microtubules into pseudopods of pseudopodial stage platelets and the complex circumferential pattern of tubule organization in outer and inner filamentous zones shown here and visualized in living platelets by VDIC-LM would also argue for microtubule reorganization, with some de- and re-polymerization as the platelet adheres and spreads on a substrate.

Acknowledgements

Supported in part by NIH Grants HL-29586 and HL 37351. The Integrated Microscopy Resource is supported as a national facility by grant #DRR570 from the Division of Research Resources of the National Institutes of Health. Monoclonal anti-tubulin was a generous gift of Dr. Steven Blose.

References

1. Albrecht RM, Olorundare OE, Bielich HW, Simmons SR. (1987). Correlative Video Enhanced DIC-LM, HVEM, and Low-Voltage High-Resolution SEM in the Study of Surface and Internal Ultrastructure. In: Proceedings of the 45th Annual Meeting of the Electron Microscopy Society of America. G.W. Bailey, (ed). San Francisco Press, Inc. pp. 556-559.

2. Faulk WP, Taylor GM. (1971). An Immunocolloid Method for the Electron Microscope. Immunocytochem., 8, 1081-1083.

3. Frens G. (1973). Controlled Nucleation for the Regulation of Particle Size in Monodisperse Gold Suspensions. Nature Phys. Sci., 241, 20-22.

4. Goodman SL, Albrecht RM. (1987). Correlative Light and Electron Microscopy of Platelet Adhesion and Fibrinogen Receptor Expression Using Colloidal Gold Labelling. Scanning Microscopy, I(2), 727-734.

5. Hodges GM, Southgate J, Toulson EC. (1987). Colloidal Gold - a Powerful Tool in Scanning Electron Microscope Immunocytochemistry: An overview of Bioapplications. Scanning Microscopy, I(1), 301-318.

6. Horisberger M. (1981). Colloidal Gold: A Cytochemical Marker for Light and Fluorescent Microscopy and for Transmission and Scanning Electron Microscopy. Scanning Electron Microsc. II, 9-31.

7. Horisberger M. (1979). Evaluation of Colloidal Gold as a Cytochemical Marker for Transmission and Scanning Electron Microscopy. Biology Cellulaire, 36, 253-258.

8. Langanger G, Moermans M, Daneels G, Sobieszek A, De Brabander M, De May J. (1986). The Molecular Organization of Myosin in Stress Fibers of Cultured Cells. J. Cell Biology 102, 200-209.

9. LangangerG, De May J, Moermans M, Daneels G, De Brabander M, Small JV. (1984). Ultrastructural Localization of a-Actinin and Filamin in Cultured Cells with Immunogold Staining (IGS) Method. J. Cell Biology 99, 1324-1334.

10. Lewis JC, White MS, Prater T, Taylor LG, Davis KS. (1982). Ultrastructural Analysis of Platelets in Nonhuman Primates. III. Stereo Microscopy of Microtubules During Platelet Adhesion and the Release Reaction. Exp. Molecular Pathology 37, 370-381.

11. Loftus JC, Albrecht RM. (1983). Use of Colloidal Gold to Examine Fibrinogen Binding to Human Platelets. Scanning Electron Microsc. IV, 1995-1999.

12. Loftus JC, Choate J, Albrecht RM. (1984). Platelet Activation and Cytoskeletal Reorganization: High Voltage Electron Microscopic Examination of Intact and Triton-Extracted Whole Mounts. J. Cell Biology 98, 2019-2025.

13. Loftus JC, Albrecht RM. (1984). Redistribution of the Fibrinogen Receptor of Human Platelets After Surface Activation. J. Cell Biol. 99, 822-829.

14. Mattson JC, Zuiches CA. (1981). The Cytoskeleton of Contact Activated Platelets. Micron 12, 69.

15. Nachmias VT. (1980). Cytoskeleton of Human Platelets at Rest and After Spreading. J. Cell Biology 86, 795-802.

16. Olorundare OE, Goodman SL, Albrecht RM. (1987). Trifluoperazine Inhibition of Fibrinogen Receptor Redistribution in Surface Activated Platelets: Correlative Video-Enhanced Differential Interference Contrast Light Microscopic, High Voltage Electron Microscopic, and Scanning Electron Microscopic Studies. Scanning Microscopy. I(2), 735-743.
17. Park K, Simmons SR, Albrecht RM. (1987). Surface Characterization of Biomaterials by Immunogold Staining - Quantitative Analysis. Scanning Microscopy, I(1), 339-350.
18. Pawley J, Albrecht R. (1988). Imaging Colloidal Gold Labels in LVSEM. Scanning. In Press.
19. Pawley J. (1984). Low Voltage SEM. J. Micros. 45, 136.
20. Pawley J. (1987). LVSEM: A New Way of Seeing Biology. In: Proceedings of the 45th Annual Meeting of the Electron Microscopy Society of America. G.W. Bailey, (ed). San Francisco Press, Inc. pp. 550-553.
21. Steiner M, Ikeda Y. (1979). Quantitative Assessment of Polymerized and Depolymerized Platelet Microtubules. Changes Caused by Aggregating Agents. J. Clin. Invest. 63, 443-448.
22. Turkevich J, Stevenson PC, Hillier J. (1951). A Study of the Nucleation and Growth Processes in the Synthesis of Colloidal Gold. Disc. Farad. Soc. 11, 55-75.
23. Walther P, Muller M. (1985). Detection of Small (5-15nm) Gold-Labelled Surface Antigens Using Backscattered Electrons. In: Science of Biological Specimen Preparation for Microscopy and Microanalysis. M. Muller, R.P. Becker, A. Boyde, and J.J. Wolosewick, (eds). Scanning Microscopy International, AMF O'Hare, Chicago, IL. pp.195-201.
24. White JG, Rao GHR. (1983). Influence of a Microtubule Stabilizing Agent on Platelet Structural Physiology. Am. J. Pathol. 112, 207-217.

Discussion with Reviewers

R. Becker: You note that the subsurface gold cannot be seen at 1 kV. Is this due to the decreased primary penetration compared to 5 kV, as you suggest, or rather is it due to the decreased yield of backscattered electrons (BE) from sub-surface gold that produce the SE II which contribute to the surface image?
Authors: Based on the work of Joy; (D. Joy, Electron Microscopy in Analysis, Institute of Physics Conference Series #90, Institute of Physics, Philadelphia and Bristol L.M. Brown Ed. 1988: 175-180) the information depth for carbon is 10 nm at 1 kV, 30 nm at 2 kV, and 100 nm at 5 kV. It is tempting to speculate in the case of the larger 18 nm particles at 1 kV, that the 10 to 15 nm coating of adsorbed protein, evaporated carbon, and contaminating hydrocarbon puts the depth of the gold just beyond the 10 nm (carbon) information depth. At 2 kV the 30 nm information depth is sufficient to allow a productive beam specimen interaction. However, the situation is borderline and sufficient beam penetration may occur at 1 kV to result in BE production from the gold core. In this case the energy of the BE is such that they would not be detectable by even the most sensitive of the commonly employed detectors. As you suggest the energy of the BE would also be such that subsequent SE II generation would be insignificant and also very difficult to detect.

In this study "subsurface" gold is not only surrounded by a layer of protein (antibody) but also is often beneath the surface, i.e., covered over by additional layers of cytoskeletal protein and cytoskeleton associated material. Hence there is very little probability of a productive primary beam-gold interaction at 1 kV accelerating voltage even if the density of the biological material is less than pure carbon. Gold label at the surface however, has only a 10-15 nm protein coat, a 3 nm carbon coat (if coated) and a small but significant contamination-related hydrocarbon coating and hence are well within the 2 kV information depth.

At 5 kV both the surface and "subsurface" particles are clearly visualized as they are within the information depth at this kV and BE of sufficient energy are generated to produce SE II.

R. Becker: What is the BE coefficient for gold at 1, 2, and 5 kV?
Authors: The accurate determination of BE coefficients at lower kVs, even in gold, will require a more complete understanding of electron-solid interactions. The most recent data available in the range of 1 kV to 10 kV suggest BE coefficients in the range of 0.3 to 0.5. Although in 2 cases a rise (1 kV to 10 kV) from 0.3 to 0.5 and 0.4 to 0.47, respectively, has been reported. A third study reported a coefficient of 0.46 as being measured across the entire range of accelerating voltages from 1.0 to 10.0 kV.

R. Becker and K. Peters: How thick was the carbon coating and was it uniformly distributed on the surface?
Authors: As you know it is difficult to judge both the thickness and distribution of a very thin carbon coat. Our best estimation based on calculation and observation is that the thickness is about 3 nm although this could be expected to vary from 1.5 to 5.0 or more nm based on geometry of the specimen.

K. Peters: At low voltage, could you resolve the tubulin fine structure on the microtubules?
Authors: No, but not for lack of resolution. These are tubules in situ. In order to preserve the integrity and organization of the entire cytoskeleton, including filaments and tubules, extraction of non-cytoskeletal material has been minimized. Hence a certain amount of microfilament and microtubule associated material remains. This does not interfere with HVEM imaging of the filaments but clearly produces an uneven coating of the various filament species and thus presents direct observation of filament fine structure at 1.0 kV. The use of more extensive extraction procedures, while compromising the overall organization of the cytoskeleton could produce relatively "clean" microtubule segments suitable for 1.0 kV imaging. Microtubules polymerized in vitro from monomeric tubulin could also provide a good "model" for 1.0 kV high resolution imaging.

K. Peters: Did you observe accumulation of contamination on your samples when working at low voltage, and did the layers of contamination reduce topographical resolution?
Authors: Yes and Yes. Even when 1. samples are dried by the critical point procedure where the alcohol and liquid CO_2 wash away many of the low molecular weight hydorcarbons which contribute to contamination, 2. when the vacuum is maintained by an oil free pumping system, and 3. when great care is taken to prevent exposure of the cleaned specimen to "dirty" room air, contamination still can be observed. When the above listed precautions are taken, contamination is significantly reduced but also appears to become more capricious. Rather than occurring all of the time, at a

fairly rapid rate wherever the beam is scanning, it occurs in some places, some of the time, at variable rates. In such a situation the contribution of "contamination" to the final image is unpredictable and difficult to evaluate. Pictures of the same point on a specimen taken after minimal scanning and again after having been scanned for various lengths of time can be compared. This is often helpful in the evaluation of "contamination". The observation of dense, uncoated, regularly shaped gold particles is also of value as comparisons of 1.0 kV and 5 or higher kV images can be used to look at the development of contamination. At 1.0 kV the surface of the contamination layer can be seen. At 5 kV the contamination layer is viewed as a halo around the central gold core. Depending on the specimen, contamination may be the major factor determining resolution.

K. Peters: At 50,000x magnification it becomes possible to measure the size of your gold probe on densely labelled microtubules. The 18 nm gold-probe can be calculated as 35 nm in diameter and the gold core coated by a 8-9 nm thick IgG layer, consistent with your results. However, the 4 nm gold-probe is 27 nm in diameter, i.e., the core must be coated by a 11 nm thick IgG layer. How then did you arrive at an IgG layer thickness of only 2 nm on the small gold probe?
Authors: The 4.0 nm size gold varies roughly from 3.0 to 5.0 nm. If one selects a number of the 0.2 nm diameter (4.0 nm) gold particles seen in figure 3c, the diameter of the core, 0.2 nm, plus the halo is approximately 0.3 to 0.4 nm. This makes the thickness of the protein coat 2 to 4 nm and the total probe diameter 6 to 8 nm. This is also what we found when the 4.0 nm beads are conjugated to antibody and spread or sprayed on a formvar film and imaged, in place, on the film. In the 1.0 kV micrograph, 3b, a number of larger approximately 25 nm spherical molecular species are present however as seen in figure 3c these are not generally associated with gold cores and probably do not represent label.